

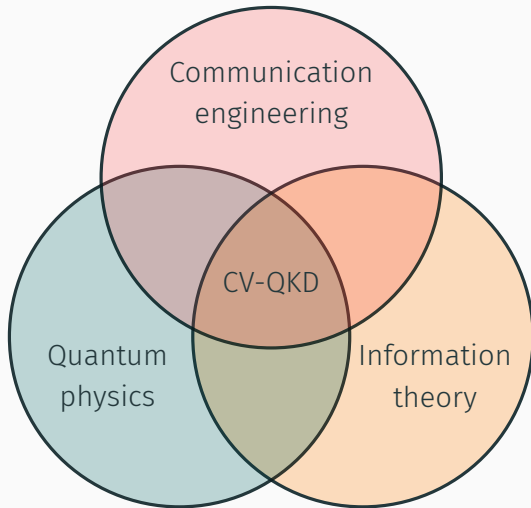
A theoretical framework for CV-QKD

Bodo Kaiser

December 7, 2021

Ludwig-Maximilians-Universität München & Huawei Munich Research Center

You never know what you might discover by thinking outside the box that culture, conformity, and critics have tried to impose. — T.D. Jakes



1. Introduction
2. Coherent state transmitter
3. Coherent state receiver
4. Conclusion and outlook

Introduction

Secure transmission system

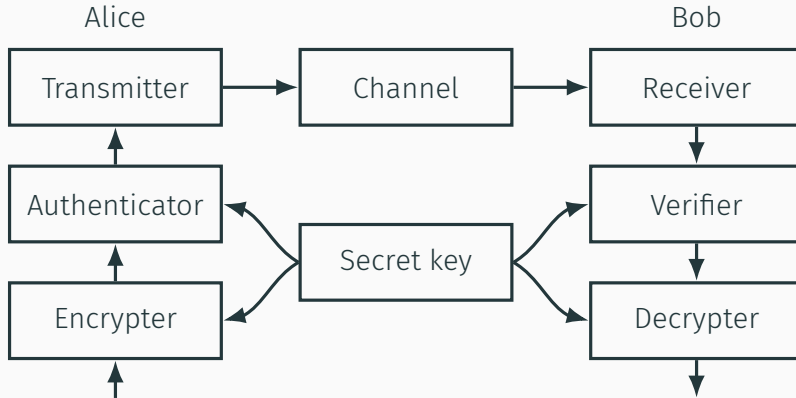


Figure 1: Block diagram of a secure transmission system.

Quantum key distribution system

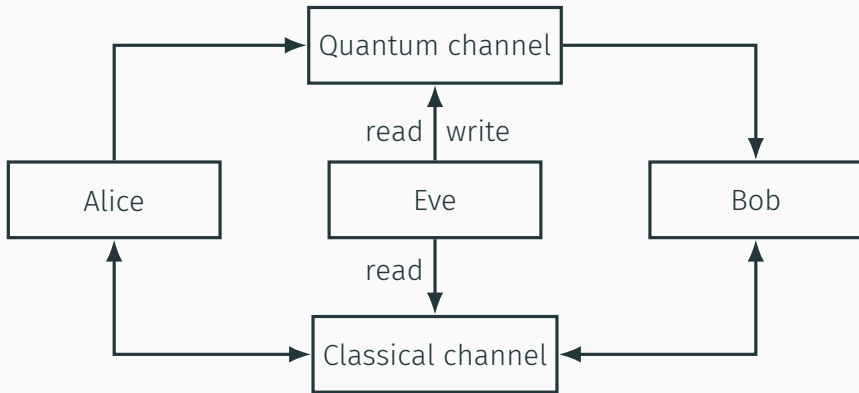


Figure 2: Block diagram of a quantum key distribution (QKD) system.

Discrete and continuous-variable QKD

Table 1: Comparison of discrete- and continuous-variable QKD.

	Discrete	Continuous
Visualization	Bloch sphere	Phase space
Hilbert space (dim)	Finite (two)	Countable (infinite)
Observable	$\hat{\mathbf{S}}(\mathbf{n}) = \hat{S}_i n^i$	$\hat{X}(\vartheta) = \frac{1}{\sqrt{2}} (\hat{a}e^{-i\vartheta} + \hat{a}^\dagger e^{+i\vartheta})$
Standard basis	$\{ 0\rangle, 1\rangle\}$	$\{ x\rangle, p\rangle\}_{x,p \in \mathbb{R}}$

Continuous-variable QKD using coherent states

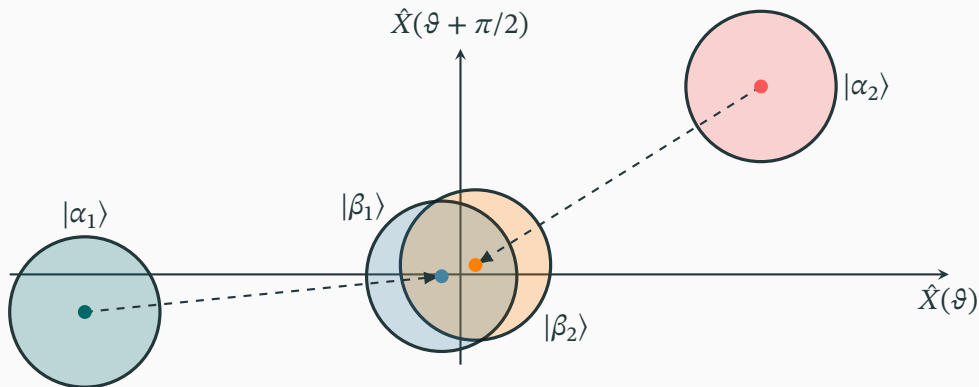


Figure 3: Phase space diagram of transmitted and received coherent states with mean (dots) and variances (opaque circles).

Continuous-variable QKD using continuous-time coherent states

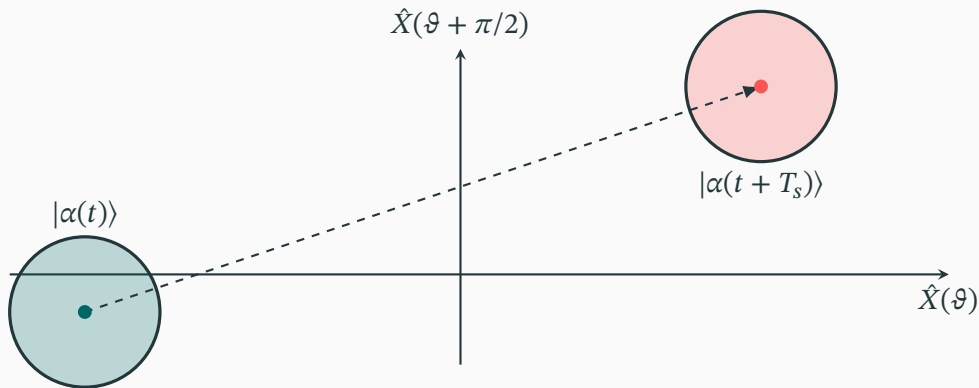


Figure 4: Phase space diagram of continuous-time coherent states with mean (dots) and variances (opaque circles) at two time instances.

Software-defined transmission system

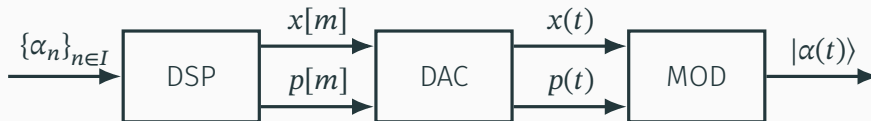


Figure 5: Block diagram of the software-defined transmitter architecture.

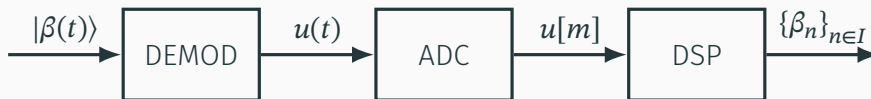


Figure 6: Block diagram of software-defined receiver architecture.

Coherent state transmitter

Digital signal processing pipeline for symbol encoding

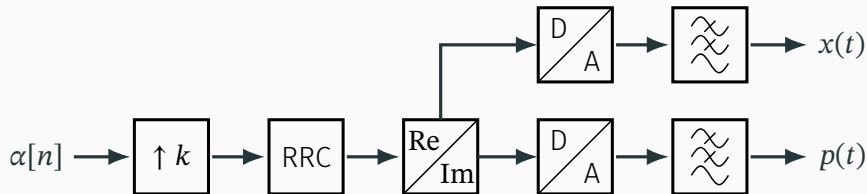


Figure 7: Block diagram of the digital signal processing for symbol encoding.

Symbol-encoding in the time domain

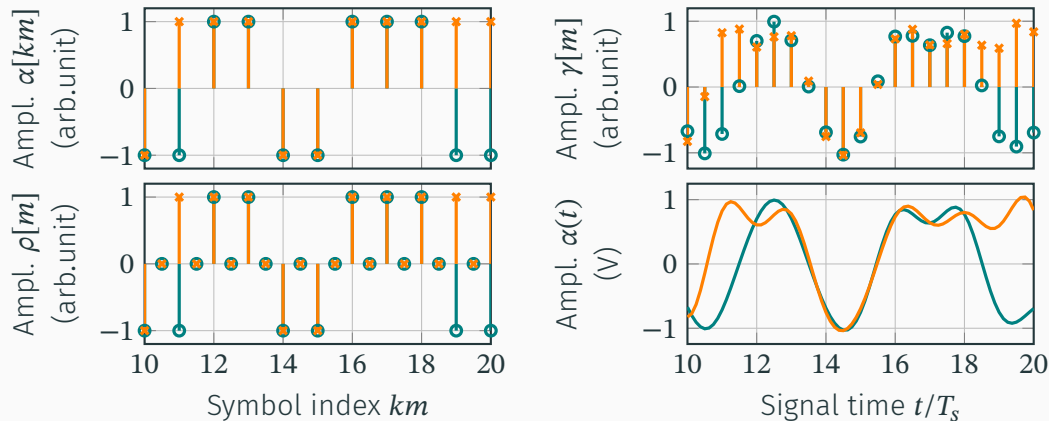


Figure 8: Symbol-encoding steps in the time domain for random QPSK sequence with real (orange) and imaginary (green) part.

Symbol-encoding steps in the frequency domain

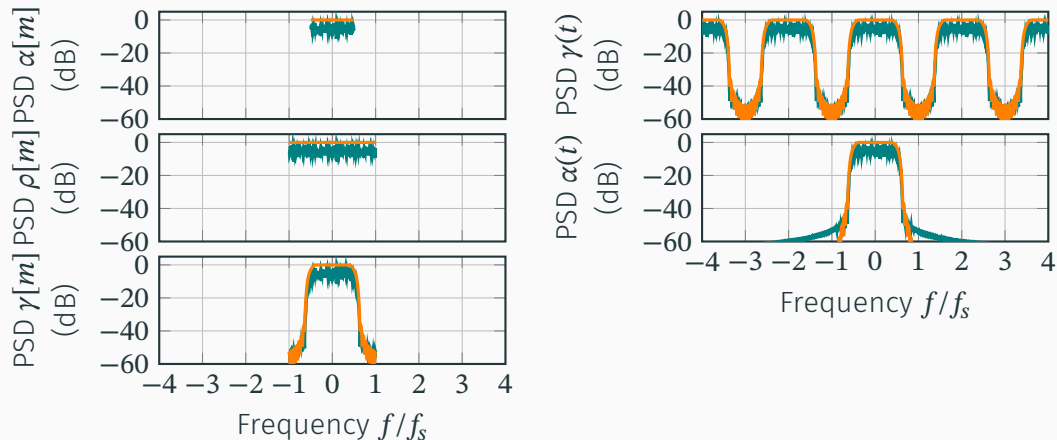


Figure 9: Symbol-encoding steps in the frequency domain for random symbols (green) and single symbol (orange).

Dual-quadrature upconversion in the time domain

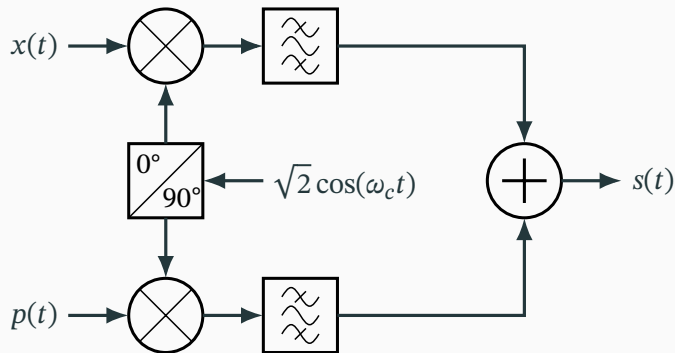


Figure 10: Power spectrum illustrating single-quadrature upconversion.

$$s(t) = x(t) \cos(\omega_c t) - p(t) \sin(\omega_c t) = \text{Re} [\alpha(t) e^{+i\omega_c t}] \quad \text{with} \quad \alpha(t) = x(t) + ip(t) \quad (1)$$

Dual-quadrature upconversion in the frequency domain

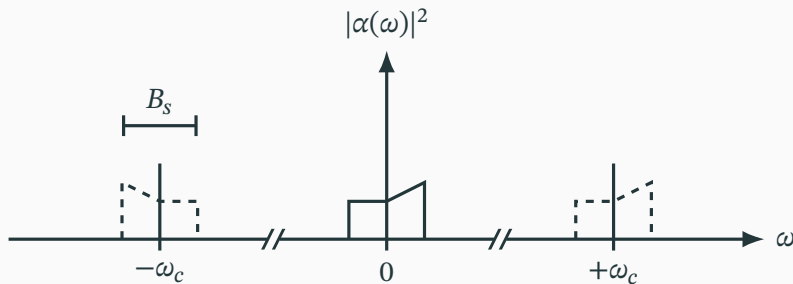


Figure 11: Power spectrum illustrating dual-quadrature upconversion.

$$s(t) = \text{Re} \int_{\omega_0 - B_s/2}^{\omega_0 + B_s/2} \frac{d\omega}{2\pi} \alpha(\omega - \omega_c) e^{+i\omega t} \quad (2)$$

In-phase and quadrature modulator as dual-quadrature upconverter

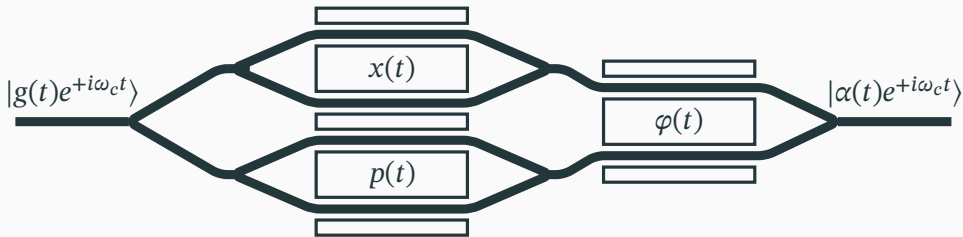


Figure 12: Drawing of an integrated in-phase and quadrature modulator.

$$|g(t)e^{+i\omega_c t}\rangle \rightarrow |\alpha(t)e^{+i\omega_c t}\rangle \quad \alpha(t) = g(t) [x(t) + iq(t)] \quad (3)$$

Interaction Hamiltonian of the electro-optical phase modulator

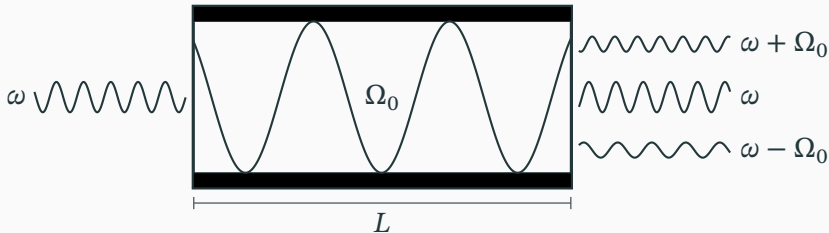


Figure 13: Traveling-wave electro-optical phase modulator of length L .

$$\hat{H}_{\text{int}} = \int \frac{d\omega}{2\pi} \int \frac{d\Omega}{2\pi} g(\omega, \Omega) \hat{a}^\dagger(\omega) \hat{a}(\Omega) \hat{a}(\omega - \Omega) + \text{H.c.} \quad (4)$$

Single-mode frequency-conversion operator

Simplifying assumptions:

- $\hat{a}(\Omega) \rightarrow \beta(\Omega)$
- $\beta(\Omega) = \beta_0 2\pi \delta^{(1)} \delta^{(1)}(\Omega - \Omega_0)$
- $\theta e^{i\varphi}/2 = \beta_0^* g(\omega, \Omega)/T$

Evolution operator:

$$\hat{U}_{\text{int}} = e^{-\frac{1}{2}\theta \hat{T}_+(\Omega_0)e^{-i\varphi} + \text{H.c.}} \quad (5)$$

Upconversion operator:

$$\hat{T}_+(\Omega_0) = \int \frac{d\omega}{2\pi} \hat{a}^\dagger(\omega + \Omega_0) \hat{a}(\omega) \quad (6)$$

$$[\hat{T}_+(\Omega_0), \hat{a}^\dagger(\omega)] = \hat{a}^\dagger(\omega + \Omega_0) \quad (7)$$

Creation operator transform:

$$\hat{U}^\dagger \hat{a}(\omega) \hat{U} = \sum_{m \in \mathbb{Z}} J_m(\theta) \hat{a}(\omega + m\omega_l) e^{-im\vartheta} \quad (8)$$

Coherent state receiver

Signal processing pipeline for symbol decoding

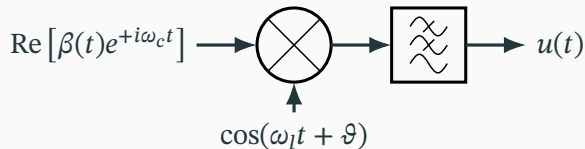


Figure 14: Block diagram of single-quadrature downconversion.

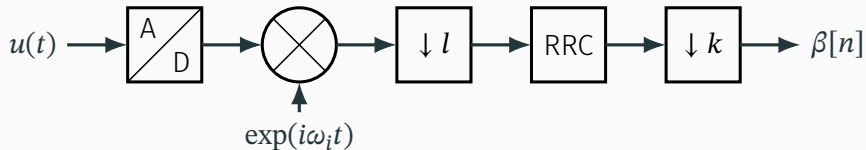


Figure 15: Block diagram of the analog-to-digital conversion and symbol-decoding.

Single-quadrature downconversion in the frequency domain

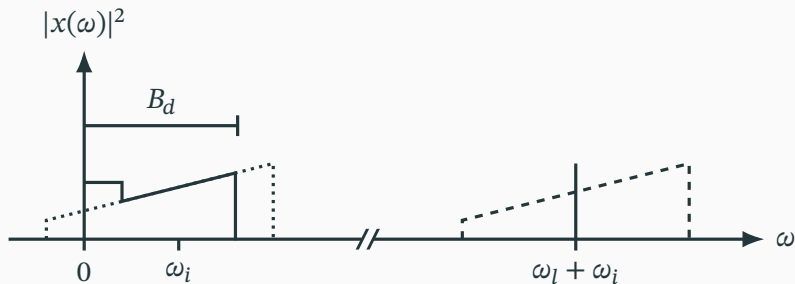


Figure 16: Power spectrum illustrating single-quadrature downconversion.

$$u(t) = \text{Re} \int_0^{+B_d/2} \frac{d\omega}{2\pi} [\beta(\omega + \omega_l)e^{+i\omega t} + \beta(\omega - \omega_l)^*e^{-i\omega t}] e^{-i\vartheta} \quad (9)$$

Single-quadrature homodyne detection

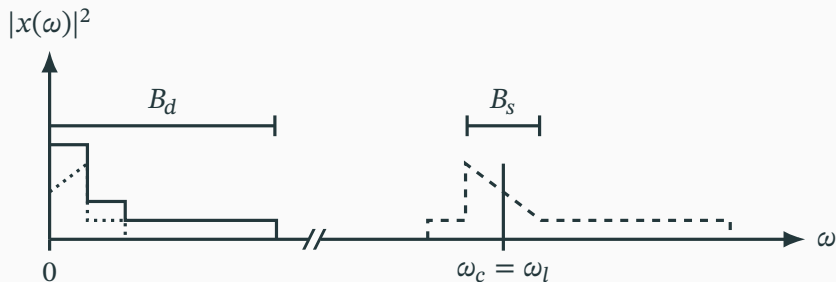


Figure 17: Power spectrum illustrating homodyne detection.

$$u(t) = \text{Re} \int_0^{+B_d/2} \frac{d\omega}{2\pi} [\beta(\omega)e^{+i\omega t} + \beta(\omega)^*e^{-i\omega t}] e^{-i\vartheta} \quad (10)$$

Single-quadrature heterodyne detection

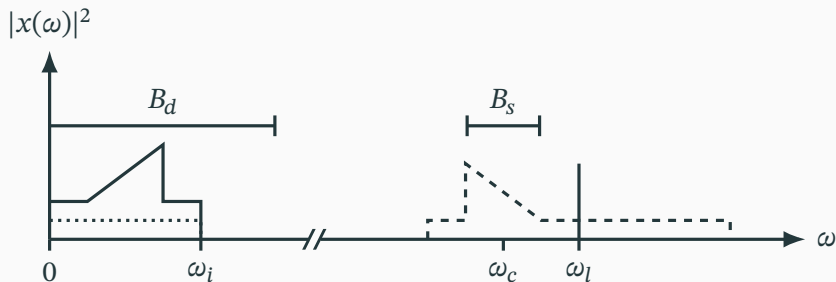


Figure 18: Power spectrum illustrating heterodyne detection.

$$u(t) = \text{Re} \int_0^{+B_d/2} \frac{d\omega}{2\pi} [\beta(\omega + \omega_i)e^{+i\omega t} + \beta(\omega - \omega_i)^*e^{-i\omega t}] e^{-i\vartheta} \quad (11)$$

Comparison homo- and heterodyne detection

Table 2: Comparison of coherent receiver designs and their implications

	Homodyne (single)	Homodyne (dual)	Heterodyne
Balanced detectors	1	2	1
Quadratures	1	2	2
Intermediate frequency	$\omega_i = 0$		$\omega_i \neq 0$
Optical complexity	Low	High	Low
Signal bandwidth	High	High	Low
LO synchronization	Frequency and phase	Frequency	Bandwidth
SNR	High	Low	Low

Balanced detector as single-quadrature downconverter

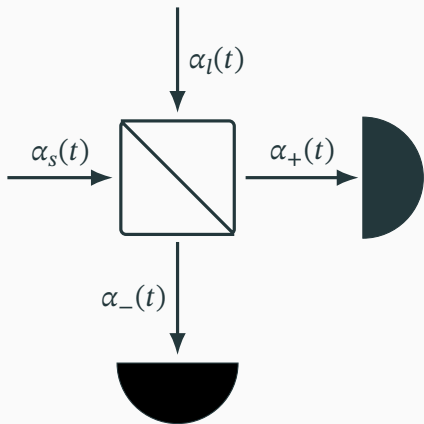


Figure 19: Electro-optical setup for balanced detection.

Differential photocurrent signal

$$i(t) \propto \text{Re} \int_{-B_d/2}^{+B_d/2} \frac{d\omega}{2\pi} \beta(\omega + \omega_l) e^{+i(\omega t + \vartheta)} \quad (12)$$

Phase-rotated quadrature operator

$$\hat{X}(t) = \int_{-\infty}^{+\infty} \frac{d\omega}{2\pi} [\hat{a}(\omega) e^{-i(\omega t + \vartheta)} + \text{H.c.}] \quad (13)$$

Frequency-converted annihilation operator

$$\hat{U}^\dagger \hat{a}(\omega) \hat{U} = \sum_{m \in \mathbb{Z}} J_m(\theta) \hat{a}(\omega + m\omega_l) e^{-im\vartheta} \quad (14)$$

Conclusion and outlook

- Introduction to CV-QKD as a mechanism for secure key distribution.
- Raised awareness to dependence of transmissions.
- Introduction to a software-defined coherent transmission system.
- Introduction to concepts and methods from communication engineering.
- Extension of coherent transmission system to quantum regime.

Additional topics covered in the thesis

- Overview and comparison of DV- and CV-QKD protocols including post processing.
- Derivation of continuous-mode quantum theory of light rooted in quantum field theory.
- Summary of quantum models for the most important (electro-)optical components as building blocks for communication system.

- Noise model for measurements.
- Comparison of image band and squeezing attack.
- Further transfer of telecommunication methods, e.g., orthogonal frequency-division multiplexing (OFDM).
- Properties of frequency-squeezed states.
- Equivalence of tensor-product with continuous-time coherent state transmission.

Maxwell equation of motion in the radiation gauge and momentum space

Free equation of motion in radiation gauge:

$$\partial_t^2 \mathbf{A} = \nabla^2 \mathbf{A} \quad A_0 = 0 \quad \partial_i A^i = 0 \quad (15)$$

Four-dimensional Fourier transform:

$$\mathbf{A}(t, \mathbf{x}) = \int \frac{d^4 p}{(2\pi)^4} \mathbf{A}(p_0, \mathbf{p}) e^{-ip_0 t + i\mathbf{p} \cdot \mathbf{x}} \quad (16)$$

Equation of motion in momentum space:

$$0 = (p_0 - \|\mathbf{p}\|)(p_0 + \|\mathbf{p}\|) \quad \omega(\mathbf{p}) = \|\mathbf{p}\| \quad (17)$$

Plane-wave and polarization basis expansion in the radiation gauge

General plane-wave expansion in radiation gauge:

$$\begin{aligned}\mathbf{A}(t, \mathbf{x}) &= \int \frac{d^4 p}{(2\pi)^3} \delta^{(1)}(p_0^2 - \omega(\mathbf{p})^2) \mathbf{A}(p_0, \mathbf{p}) e^{-ip_0 t + i\mathbf{p} \cdot \mathbf{x}} \\ &= \int \frac{d^4 p}{(2\pi)^3 \sqrt{2\omega(\mathbf{p})}} \mathbf{A}(\omega(\mathbf{p}), \mathbf{p}) e^{-ip_0 t + i\mathbf{p} \cdot \mathbf{x}} + \text{h.c.}\end{aligned}\tag{18}$$

Polarization basis expansion

$$\mathbf{A}(t, \mathbf{x}) = \sum_{\lambda=1,2} a_{\lambda}(\mathbf{p}) \hat{\mathbf{e}}_{\lambda}(\mathbf{p})\tag{19}$$

Polarization basis transverse to momentum:

$$\mathbf{p} \cdot \hat{\mathbf{e}}_{\lambda}(\mathbf{p}) = 0 \quad \hat{\mathbf{e}}_{\lambda}(\mathbf{p}) \hat{\mathbf{e}}_{\sigma}(\mathbf{p}) = \delta_{\lambda,\sigma} \quad \sum_{\lambda=1,2} \hat{\mathbf{e}}_{\lambda}(\mathbf{p})^i \hat{\mathbf{e}}_{\lambda}(\mathbf{p})^j = \delta^{ij} - \frac{p^i p^j}{\mathbf{p}^2}\tag{20}$$

Canonical quantization in the Coulomb gauge

Conjugate momentum density:

$$\Pi_i = \partial_t A_i = E_i = -E^i \quad (21)$$

Equal-time commutation relations:

$$[\hat{A}_i(t, \mathbf{x}), \hat{E}_j(t, \mathbf{y})] = -i\delta_{\perp,ij}^{(3)}(\mathbf{x} - \mathbf{y}) \quad (22)$$

$$[\hat{A}_i(t, \mathbf{x}), \hat{A}_j(t, \mathbf{y})] = [\hat{E}_i(t, \mathbf{x}), \hat{E}_j(t, \mathbf{y})] = 0 \quad (23)$$

Transverse delta distribution:

$$\delta_{\perp,ij}^{(3)}(\mathbf{x} - \mathbf{y}) = \left(\delta_{ij} - \frac{\partial_i \partial_j}{\partial^2} \right) \delta^{(3)}(\mathbf{x} - \mathbf{y}) = \int \frac{d^3 p}{(2\pi)^3} \left(\delta_{ij} - \frac{p_i p_j}{\mathbf{p}^2} \right) e^{i\mathbf{p} \cdot \mathbf{x}} \quad (24)$$

Maxwell field operators

Negative-frequency Maxwell field operator

$$\mathbf{A}^{(-)}(t, \mathbf{x}) = \sum_{\lambda=1,2} \int \frac{d^3p}{(2\pi)^3 \sqrt{2\omega(\mathbf{p})}} \hat{a}_{\lambda}(\mathbf{p}) \hat{\mathbf{e}}_{\lambda}(\mathbf{p}) e^{-i\omega(\mathbf{p})t + i\mathbf{p} \cdot \mathbf{x}} \quad (25)$$

Negative-frequency electric field operator

$$\mathbf{E}^{(-)}(t, \mathbf{x}) = -i \sum_{\lambda=1,2} \int \frac{d^3p}{(2\pi)^3 \sqrt{2\omega(\mathbf{p})}} \omega(\mathbf{p}) \hat{a}_{\lambda}(\mathbf{p}) \hat{\mathbf{e}}_{\lambda}(\mathbf{p}) e^{-i\omega(\mathbf{p})t + i\mathbf{p} \cdot \mathbf{x}} \quad (26)$$

Hamiltonian and momentum operator

$$\hat{H} = \sum_{\lambda=1,2} \int \frac{d^3p}{(2\pi)^3} \omega(\mathbf{p}) \hat{a}_{\lambda}^{\dagger}(\mathbf{p}) \hat{a}_{\lambda}(\mathbf{p}) \quad \hat{\mathbf{P}} = \sum_{\lambda=1,2} \int \frac{d^3p}{(2\pi)^3} \mathbf{p} \hat{a}_{\lambda}^{\dagger}(\mathbf{p}) \hat{a}_{\lambda}(\mathbf{p}) \quad (27)$$

Axiomatic particle state construction

Vacuum state

Poincare invariance:

$$\hat{U}(a, \Lambda)|0\rangle = |0\rangle \quad (28)$$

Implies zero energy and momentum:

$$\hat{H}|0\rangle = 0|0\rangle \quad \hat{\mathbf{P}}|0\rangle = \mathbf{0}|0\rangle \quad (29)$$

Implies annihilation operator destroying vacuum:

$$\hat{a}(\mathbf{p})|0\rangle = 0 \quad (30)$$

Momentum state

Algebraic commutation relations:

$$[\hat{N}, \hat{a}^\dagger(\mathbf{p})] = \hat{a}^\dagger(\mathbf{p}) \quad (31)$$

$$[\hat{\mathbf{P}}, \hat{a}^\dagger(\mathbf{p})] = \mathbf{p}\hat{a}^\dagger(\mathbf{p}) \quad (32)$$

Implies eigenstates:

$$\hat{N}\hat{a}^\dagger(\mathbf{p})|0\rangle = 1\hat{a}^\dagger(\mathbf{p})|0\rangle \quad (33)$$

$$\hat{\mathbf{P}}\hat{a}^\dagger(\mathbf{p})|0\rangle = \mathbf{p}\hat{a}^\dagger(\mathbf{p})|0\rangle \quad (34)$$

but not normalizable

$$\langle 0|\hat{a}(\mathbf{p})\hat{a}^\dagger(\mathbf{p})|0\rangle = (2\pi)^3\delta^{(3)}(\mathbf{p} - \mathbf{q}) \quad (35)$$

Smeared single-particle state

Interpretation as quantum operators as distributions:

$$\hat{A}^{(+)}[f]|0\rangle = \int d^4x f(t, \mathbf{x}) \hat{A}^{(+)}(t, \mathbf{x}) = \int \frac{d^3p}{(2\pi)^3} \frac{f(\omega(\mathbf{p}), \mathbf{p})}{\sqrt{2\omega(\mathbf{p})}} \quad (36)$$

Normalizable iff:

$$\langle 0 | \hat{A}^{(-)}[f] \hat{A}^{(+)}[f] | 0 \rangle = \int \frac{d^3p}{(2\pi)^3} \left| \frac{f(\omega(\mathbf{p}), \mathbf{p})}{\sqrt{2\omega(\mathbf{p})}} \right|^2 = 1 \quad (37)$$

Implies eigenstates:

$$\hat{N} \hat{A}^{(+)}[f]|0\rangle = 1 \hat{A}^{(+)}[f]|0\rangle \quad \hat{H} \hat{A}^{(+)}[f]|0\rangle = \int \frac{d^3p}{(2\pi)^3} \omega(\mathbf{p}) \left| \frac{f(\omega(\mathbf{p}), \mathbf{p})}{\sqrt{2\omega(\mathbf{p})}} \right|^2 \hat{A}^{(+)}[f]|0\rangle \quad (38)$$

Generalized number and coherent state

Number state

$$|n_f\rangle = \frac{1}{\sqrt{n!}} \hat{A}^{(+)} [f]^n |0\rangle \quad (39)$$

Mean energy:

$$n \int \frac{d^3 p}{(2\pi)^3} \omega(\mathbf{p}) \left| \frac{f(\omega(\mathbf{p}), \mathbf{p})}{\sqrt{2\omega(\mathbf{p})}} \right|^2 \quad (40)$$

Electric field at (t, \mathbf{x}) :

$$0 \pm \frac{1}{2} \int \frac{d^3 p}{(2\pi)^3} \omega(\mathbf{p}) + n |\Psi(t, \mathbf{x})|^2 \quad (41)$$

Coherent state

$$|\alpha\rangle = \exp \{ \hat{A}^{(+)} [\alpha] - \text{H.c.} \} |0\rangle \quad (42)$$

Mean energy:

$$\int \frac{d^3 p}{(2\pi)^3} \omega(\mathbf{p}) \left| \frac{\alpha(\omega(\mathbf{p}), \mathbf{p})}{\sqrt{2\omega(\mathbf{p})}} \right|^2 \quad (43)$$

Electric field at (t, \mathbf{x}) :

$$0 \pm \frac{1}{2} \int \frac{d^3 p}{(2\pi)^3} \omega(\mathbf{p}) \quad (44)$$

Connection to continuous-mode quantum optics

Central assumption

No relative motion, i.e., no Lorentz boosts.

Typical approximations:

- Neglect polarization degrees of freedom
- Neglect transverse momentum distribution
- Neglect relativistic Lorentz factor $1/\sqrt{2\omega}$

Phase-rotated quadrature operator:

$$\hat{X}(t) = \frac{1}{\sqrt{2}} \int \frac{d\omega}{2\pi} \left\{ \hat{a}(\omega) e^{-i(\omega t + \vartheta)} + \text{H.c.} \right\} \quad (45)$$

Maxwell field at (t, \mathbf{x}) :

$$\hat{A}(t, \mathbf{x}) = \int \frac{d\omega}{2\pi\sqrt{2\omega}} \left\{ \hat{a}(\omega) e^{-i\omega(t-x)} + \text{H.c.} \right\} \quad (46)$$